

III-nitride micro-emitter arrays: development and applications

This article has been downloaded from IOPscience. Please scroll down to see the full text article.

2008 J. Phys. D: Appl. Phys. 41 094001

(<http://iopscience.iop.org/0022-3727/41/9/094001>)

View [the table of contents for this issue](#), or go to the [journal homepage](#) for more

Download details:

IP Address: 129.118.86.52

The article was downloaded on 09/08/2010 at 19:32

Please note that [terms and conditions apply](#).

INVITED PAPER

III-nitride micro-emitter arrays: development and applications

Z Y Fan, J Y Lin and H X Jiang

Department of Physics, Kansas State University, Manhattan, KS 66506-2601, USA

E-mail: jiang@phys.ksu.edu

Received 1 October 2007

Published 4 April 2008

Online at stacks.iop.org/JPhysD/41/094001**Abstract**

III-nitride micro-emitter array technology was developed in the authors' laboratory around 1999. Since its inception, much progress has been made by several groups and the technology has led to the invention of several novel devices. This paper provides an overview on recent progress in single-chip ac-micro-size light emitting diodes (μ LEDs) that can be plugged directly into standard high ac voltage power outlets, self-emissive microdisplays and interconnected μ LEDs for boosting light emitting diodes's wall-plug efficiency, all of which were evolved from III-nitride micro-emitter array technology. Finally, potential applications of III-nitride visible micro-emitter arrays as a light source for DNA microarrays and future prospects of III-nitride deep ultraviolet micro-emitter arrays for label-free protein analysis in microarray format by taking advantage of the direct excitation of intrinsic protein fluorescence are discussed.

(Some figures in this article are in colour only in the electronic version)

1. Introduction

Significant progress in nitride material technology has been achieved leading to commercially available high performance visible and near ultraviolet (UV) light emitting diodes (LEDs) and near UV laser diodes (LDs) based on III-nitrides. The recent success of the III-nitride edge-emitters and detectors is encouraging for the study of micro-size photonic structures and devices. These micro-photonic devices range from arrays of micro-emitters, detectors and waveguides to optical switches and photonic crystals. New physical phenomena and properties begin to dominate as the device size scale approaches the wavelength of light, including modified spontaneous emission, enhanced quantum efficiency and lasing in microcavities, all of which warrant fundamental investigations. The unique properties of III-nitrides, including UV/blue/green emission, the ability to operate at very high temperatures and power levels and the ability of band gap engineering through alloying and heterostructures, may allow the creation of micro-size optoelectronic and photonic devices with unprecedented properties and functions.

The micro- and nano-photonic technologies, similar to the integration of Si transistors in the 1960s, are expected

eventually to provide the ability to integrate arrays of thousands of cheaply fabricated optical circuit elements such as light sources, detectors, waveguides, switches and resonator on a single chip. Together with their potential for optical circuit elements integration, these micro-photonic devices are expected to open many important applications such as optical communications, signal and image processing, optical interconnects, computing, enhanced energy conversion and storage, chemical, biohazard substance and disease detection. The physics of micro-size photonic structures and devices has been investigated and much progress has been made in the last decade. Nitride micro-photonic structures, including micro-size discs, rings, pyramids, prisms and optically-pumped vertical cavity surface emitting laser (VCSEL) structures with feature sizes down to sub-micrometres, have also been studied by several groups [1–10]. All prior results point to the superior properties of III-nitride micro-phonics. However, it is only recently that a transition from basic research to practical device components has been made for III-nitride micro-size photonic devices due to various technological advances. Following the report [11, 12] of the first current-injected InGaN micro-size light-emitting diodes (μ LEDs) and μ LED array, different groups [13–16] have been pursuing this new concept. Several

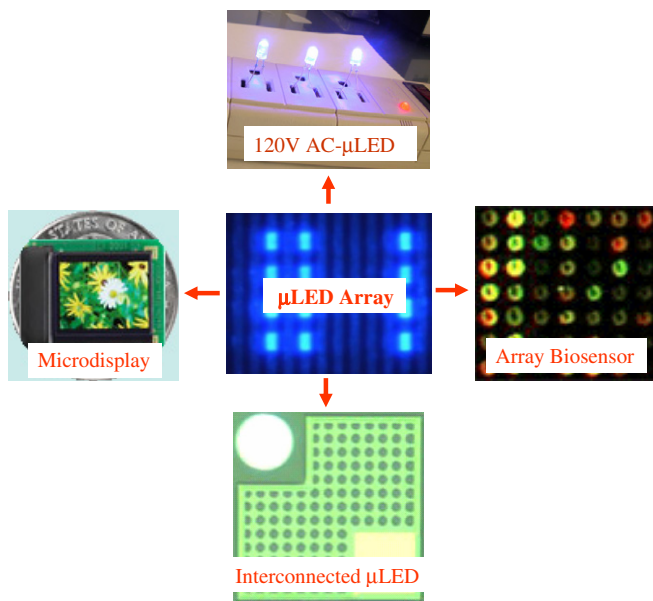


Figure 1. New devices evolved from III-nitride μ -emitter array technology, including single-chip ac-LEDs that can be plugged directly into standard high ac voltage power outlets, parallel interconnected μ LEDs for boosting the extraction efficiency of LEDs, matrix addressable μ LED array for emissive microdisplays and III-nitride μ LED array based biosensors.

novel practical devices, as illustrated in figure 1, have been evolved from III-nitride μ -emitter array technology. This paper provides an overview on the recent developments of the emerging III-nitride μ -emitter array based devices. These include single-chip ac- μ LEDs that can be plugged directly into standard high ac voltage power outlets, semiconductor self-emissive microdisplays, interconnected μ LEDs for boosting LED's wall-plug efficiency and III-nitride visible micro-emitter array based biochip arrays. Finally, future prospects of III-nitride deep UV micro-emitter array for label-free protein analysis in microarray format by taking advantage of the direct excitation of intrinsic protein fluorescence are discussed.

Section 2 briefly describes the III-nitride μ -emitter material structure, fabrication process and basic characteristics. Section 3 discusses the emerging III-nitride AC- μ LED technology for general lighting (or solid-state lighting) applications. Section 4 reviews the results of the interconnected μ LED approach to significantly enhance the extraction efficiency of III-nitride LEDs. In section 5, the achievement of III-nitride based self-emissive microdisplay is described. In section 6, the prospects of nitride μ -emitter array for biological and medical sensor applications are discussed.

2. Micro-emitter structure, process and characterization

Like III-nitride LEDs, most μ -emitter structures discussed in this paper were grown on (0001) sapphire substrates by metal-organic chemical vapour deposition (MOCVD). The insulative sapphire substrate provides an ideal platform for the isolation between individual μ LEDs. All the emitter structures are based on multi-quantum wells (MQWs) confined between

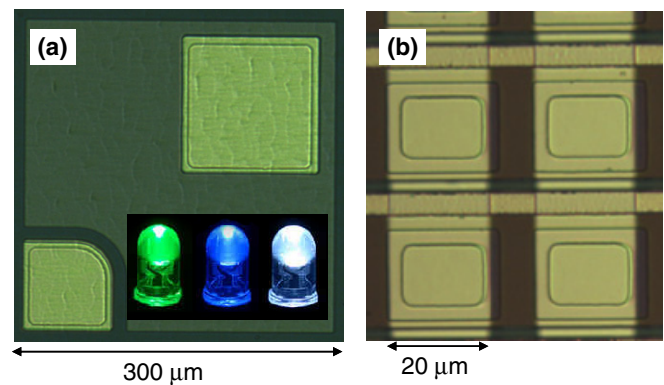


Figure 2. Comparison of conventional LEDs and μ LEDs. Microscope images of (a) a conventional broad-area LED with a device size of $300\ \mu\text{m} \times 300\ \mu\text{m}$ (inset shows the encapsulated LED lamps) and several μ LEDs with a device size of $20\ \mu\text{m} \times 20\ \mu\text{m}$ fabricated by the authors' group.

n-type and p-type barriers. The emission wavelength is tuned by adjusting In and Al compositions in the AlInGaN alloy of the MQW active region. For visible wavelength, n- and p-GaN are the barrier layers, and for UV wavelength, n- and p-AlGaIn are the barrier layers.

As illustrated in figure 2, the conventional broad-area LED has a typical device area of $300\ \mu\text{m} \times 300\ \mu\text{m}$ and is encapsulated into the standard 3 mm or 5 mm lamps, while a μ LED has an active mesa size from about $50\ \mu\text{m}$ down to several micrometres, limited by the p-contact area. A typical nitride μ LED has a mesa structure with the n- and p-contacts fabricated on the same side because of the insulating sapphire substrate. The process starts from the blank deposition of Ni/Au metals on the p-GaN surface with an e-beam evaporator. Plasma etch is used to etch into n-GaN to form a circular or rectangular mesa, then another plasma etch is taken down to the sapphire substrate. After thermal annealing in air, the oxidized Ni/Au alloy forms a transparent contact on p-GaN with a transmission of 70–75% at visible wavelength. Ti/Al metal stack is deposited on n-GaN to form n-type ohmic contacts. After a SiO_2 insulation layer is conformably deposited by plasma-enhanced chemical vapour deposition (PECVD) on the mesa sidewalls to isolate the n-GaN, a Ni/Au stack is deposited as a p-pad. Surface passivation may also be used as a last step for protection.

An inductively-coupled plasma (ICP) is used to define the μ LED mesa structure. Surface damage introduced by plasma etch will enhance the nonradiative recombination rate, especially for the μ LED with a large surface area as compared with its bulk volume. Special steps for surface treatments, including chemical wet etching after plasma etch and oxide/polymer surface passivation to remove the damage and compensate for the dangling bonds, can be adopted in the process. Controlling the etch profile is also critical.

The μ LED is much more efficient than the broad-area LED, and a power density enhancement up to five times has been obtained by different groups [17, 18]. The enhanced extraction efficiency of μ LED has been utilized to boost the LED efficiency. Based on time-resolved electrical luminescence (EL) measurement, it was found that μ LED has

a very fast response [17]. The measured turn-on time is on the order of tens of picoseconds. The operating speed of a μ LED is limited by its turn-off time and increases with a decrease in the μ LED size. The response time reduced from 0.21 ns for devices with a diameter (d) of 15 μ m to 0.15 ns for $d = 8 \mu$ m. This property ensures that the μ LED based nitride microdisplay has a much faster response than LCD and OLED based microdisplays. Another critical application of III-nitride μ -emitters is for bio-molecule intrinsic fluorescence property measurements. The fast operating time of III-nitride μ -emitters also ensures that these devices are perfect light sources for fluorescence lifetime measurements of medical and biological samples.

3. Single-chip ac-LEDs based on III-nitride μ LED arrays

Currently, about 21% of electricity is used for lighting and the most widely used sources of artificial illumination are incandescent and fluorescent lamps, an industry that has changed very slowly since the 19th century. If used in place of incandescent light bulbs, LEDs based solid-state lighting (SSL) would provide compactness, longer lifetimes (>20 000 h for LEDs compared with 2000 h for incandescent light bulbs), while consuming only a fraction of the electrical power for the same luminous intensity because all of the light produced is used, not wasted in the form of heat, resulting in significant energy and maintenance man-hour savings. Additional associated benefits include reduced oil imports, lower greenhouse gas emissions and lower energy costs to consumers. Because of the enormous potential for energy savings, as well as environmental benefits, there is currently great interest worldwide in developing new technologies that would bring the potentials of SSL to reality.

All conventional semiconductor LEDs are operated under dc current with typical operating voltages of a few volts (e.g. around 2 V for red LEDs and around 3.2 V for blue LEDs). Nonetheless, all the houses and buildings in the world are wired with ac (60 or 50 Hz) 110 V (or 220 V) power sources. One way to use LEDs for general lighting and illumination applications is to convert ac high voltage to dc low voltage. This requires the use of power converters or RC circuits, which can be installed separately or built into the LED package. This approach has been utilized in LED traffic signal lights and also in some 120 V/220 V ac-LED replacement bulbs distributed by many vendors. It is obvious that power converters or RC circuits have disadvantages such as added volume (bulky) and costs, reduced efficiency and limited current supply. There is also an obvious method for achieving the 'ac operation' by wiring together a strand of discrete LEDs, but it would not be economically or/and physically viable to replace an incandescent lamp by a strand of discrete LEDs—one needs to connect a few dozens of LEDs to achieve high voltage ac operations.

In recent years, ac-driven LED lamps have also been developed based on capacitance coupling. In this design, a capacitor is selected with suitable impedance to limit the current flowing through the conventional LED, as shown in figure 3. Comparing with the ac-dc transforming scheme,

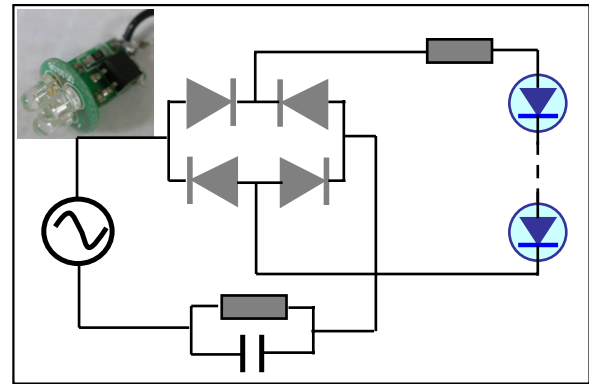


Figure 3. Schematic circuit of capacitor coupling based ac-driven LEDs, with the inset image showing such a lamp.

this capacitor coupling design has higher efficiency, but some power is still lost on the current limiting and discharging resistors, and more critically, the huge rush-in transit current can easily blow off the LED, causing serious safety problems. It is recognized by the LED community that fundamental advancements and innovations associated with chip-level architectures are the key to bring SSL to reality, analogous to the Si integrated circuit (IC) technology for electronics.

III-N technology (3N) has developed, based on μ LED technology, single-chip ac-LEDs that can be plugged directly into standard power outlets or lamp sockets without power conversion and without external RC circuits [19]. The 3N's invention evolved from the μ LED array technology initially developed by the authors. The 3N's single-chip ac-LEDs integrate arrays of μ LEDs on-chip for high voltage ac operation. The number of linked emitters is chosen so that the sum of the voltage drops across the individual emitters adds up to the voltage of the ac supply. Since LEDs only emit light when they are forward biased, two arrays are created, one of which lights up during the first half cycle of the ac power source and the other which lights up when the polarity of the source is reversed. Compared with other existing/competing technologies, the serial integration of μ LED array on-chip avoids multiple soldering points. Furthermore, with two reverse LED arrays corresponding to the current flow of the positive and negative half cycles of ac voltage, the light on/off frequency is doubled from 50–60 Hz VAC frequency to 100–120 Hz, and eye uncomfartableness by light flickering is eliminated. Like the dc power-LEDs targeting for lighting applications, flip-chip bonding may also be applied to single-chip ac-LED to enhance thermal conduction, to increase light collection and especially to transfer the interconnection metal wires to the flat submount surface [20].

Based on the invention of single-chip ac-LEDs, 3N further developed the μ LED based low power indicator ac- μ LED lamps. Depending on the driving voltage 120 V ac or 220 V ac, a certain number of μ LEDs are integrated on a single chip, with the chip size and power consumption comparable to those of the standard LED indicator devices, so that the ac- μ LED array chip can be directly packaged in the housing used for the standard LED indicator lamp. The result is a high voltage ac indicator lamp with the same or similar outside features as

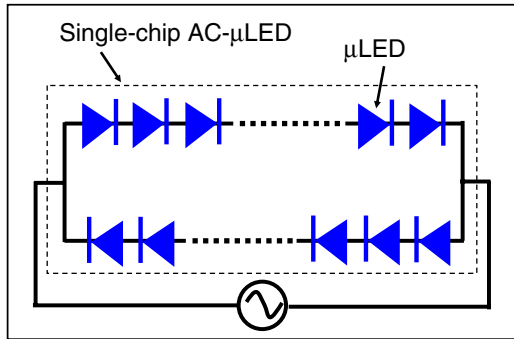


Figure 4. The principle of single-chip ac-μLEDs based on two serial arrays of μLEDs with reverse current flowing direction (after [19]).

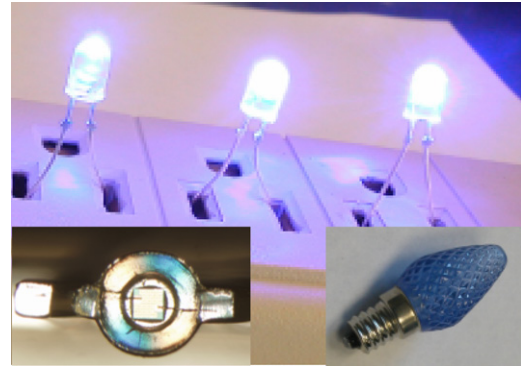
the standard LED indicator lamp. Depending on the detailed design, the supplied power to the high voltage inductor lamp may be an ac voltage such as 110/120 V and 220/240 V, or high dc voltages.

Figure 4 illustrates the basic principle of ac-μLEDs. A certain number of μLEDs are connected in series—the p-contact of one μLED is connected with the n-contact of its neighbouring μLED; the result is that the applied voltage to the array equals the sum of the voltage drop on each μLED. Two arrays are parallelly connected, but they are arranged to have a reversed current flow direction, so that in each half cycle, there is one array emitting light. In this scheme, a conventional LED (with a size of 0.3 mm × 0.3 mm) may be replaced by an ac-μLED for 120 V ac.

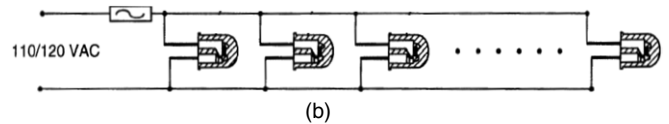
The insulating sapphire substrate provides a suitable base for the isolation of individual μLEDs. For the LED structure grown on conductive SiC or Si substrates, the isolation approach is to incorporate a layer of insulating material between the substrate and the LED structure. For InGaN LED, the AlN/sapphire template has been demonstrated to be superior to the GaN buffer for LED efficiency by reduction of threading dislocations and enhancement of thermal conductivity [21]. For silicon substrates, the AlN layer has to be used to avoid wafer bowing and crack in the LED structure [22]. Highly insulating AlN also provides an ideal layer for μLED isolation.

Ac-μLEDs with the same device area as dc LEDs have been fabricated. Under the same input power, dc and ac-μLED provide similar efficiency. ac-μLED chips can easily fit into the standard T1 and T1-3/4 lead-frames. Figure 5(a) is the image of packaged 5 mm indicator AC-μLED lamps directly plugged in the 120 V ac power outlets. The left inset shows the ac-LED die mounted in the reflecting cup of the package lead-frame, and the right inset shows that the 5 mm or the 3 mm lamp is inserted in a screw based C6 package with a strong protecting shell to improve reliability and safety. The input power of the 120 V ac indicator lamp is less than the maximum limitation of the standard LED package, ensuring its reliability without overheating.

One of the immediate applications of the ac-μLED indicator lamp is for indication and signalling purposes with a direct connection to the 120 V ac power supply. As an example for Christmas tree decorations, a parallel ac-μLED lamp



(a)



(b)

Figure 5. (a) The picture shows the packaged ac-μLEDs (fabricated by the authors) directly driven by 120 V ac power outlets. The left inset shows an ac-μLED die in the reflection cup, and the right inset shows 3 mm or 5 mm ac-μLED lamp inserted in the C6 package for protection. (b) Schematic shows an ac-μLED with the C6 package being connected in parallel to construct LED string directly driven by the ac line voltage (courtesy: III-N Technology, Inc.)

string may be constructed based on the strong C6 package, as illustrated in figure 5(b). Since each lamp runs with very low current, there is almost no limitation on the number of lamps connected in the string, and the string can be directly plugged into the household ac power supply without any transformer, rectifier or RC circuits.

4. Interconnected μLED array for boosting LED emission efficiency

Most light generated in a LED tends to be trapped in the semiconductor by total internal reflection, with an escaping angle of only $(1/4n^2) \times 4\pi$ steradians. Semiconductors have a high refractive index, which is 2.5 for GaN and 3.4 for AlGaInP. Such a high refractive index limits the photon extraction efficiency of conventional planar InGaN LEDs to less than ~5% by total internal reflection. The light-trapping problem is more serious for power LEDs with larger die areas for solid-state lighting applications, because less light can be extracted from the peripheral sidewalls of large dies. Many approaches have been proposed and demonstrated to enhance light extraction. Die shaping has been widely studied since the infancy of LED technology in the 1960s, and the truncated inverted pyramid (TIP) LED is an example of an LED employing advanced die shaping to enhance the external efficiency of an AlInGaP/GaP red LED by 1.4 times [23], but the sawing process for die shaping is not suitable for GaN hard materials. Surface roughening or textured semiconductor surface [24], micro-lens array [25] and photonic crystals [26] all have been demonstrated to increase the light extraction efficiency.

Another approach to boost the LED power output by replacing conventional broad-area LEDs with hundreds of

μ LEDs in parallel connection have been demonstrated [27]. The novel architecture interconnects hundreds of μ LEDs (size on the order of $10\ \mu\text{m}$ in diameter). These interconnected μ LEDs fit into the same device area as a conventional broad-area LED of $300 \times 300\ \mu\text{m}^2$. It was shown that for interconnected μ LEDs, the overall emission efficiency was increased over the conventional LEDs for the same device area.

Interconnected μ LEDs with different individual micro-disc diameters were fabricated by photolithographic patterning and ICP dry etching. A transparent film of Ni/Au was deposited to connect the p-type ohmic contacts of each individual μ LEDs in a net-like configuration. The processing steps are identical to those of the conventional broad-area LEDs. The I - V characteristics of interconnected μ LEDs and a conventional broad-area LED fabricated from the same wafer were compared. The forward bias voltages at 20 mA, V_F , for the two types of LEDs are comparable and are about 3.7 V for 408 nm LEDs. The EL spectral shapes of the interconnected μ LEDs and the conventional broad-area LED are quite similar. The light power output versus forward current (L - I) for an interconnected μ LED of disc diameters of $d = 12\ \mu\text{m}$ and for a conventional broad-area LED is compared. Intriguingly, the results demonstrate that the power output increases by about 50% at 20 mA in the interconnected μ LED over the conventional broad-area LED, despite the fact that the total active area of an interconnected LED is reduced compared with a broad-area LED of the same device area. In a similar study, Choi *et al* [28] reported the performance of an InGaN LED based on interconnected the micro-ring device array, and it was demonstrated that under the same emission area, the micro-ring array gives more light than the micro-disc array, which was explained based on the argument that the micro-ring has inner and outside mesa walls for light extraction.

The features of interconnected μ LEDs are particularly beneficial to UV emitters as the light extraction becomes even more difficult in UV wavelength [29]. For 340 nm UV LEDs [30], the interconnected μ LED architecture provides enhanced power output at all input currents due to enhanced extraction efficiency and current density. Adivarahan *et al* adopted the interconnected μ LED architecture for 280 nm deep UV LEDs by introducing additional interconnection between n-contacts of μ LEDs [31]. It was argued that for typical 280 nm DUV LEDs, limited by the high sheet resistance of the bottom n-AlGaIn contact layer, the current spreading length is only 30–40 μm . Comparing with the multi-narrow-strip geometry with interdigitated n-contact fingers, an interconnected μ LED design can offer a 2D reduction in both the series resistance and thermal impedance for large peripheral DUV LEDs. An interconnected 10×10 pixel array with each pixel of 26 μm diameter has a differential resistance of 9.8 Ω , while it is 40 Ω for a $100 \times 100\ \mu\text{m}^2$ LED. At low current, the interconnected pixel design gives a lower output power because the nonradiative recombination pathways strongly limit the device quantum efficiency, while at high current after these pathways are saturated, the pixel design gives a peak power of 50% increase over other square geometries because of its superior light extraction, current uniformity and low thermal impedance. A similar scheme was also applied by the same group to 254 nm DUV LEDs [32].

5. Self-emissive microdisplays based on III-nitride μ LED arrays

As illustrated in figure 6, microdisplays have a small size typically less than 1 inch diagonal with a resolution from the low end of 1/4 QVGA to above the XVGA format. They are magnified by optics to form an enlarged virtual image or a projected image and can be used in a variety of devices such as head-mounted displays, video headsets, camcorder viewfinders, projection TV and head-up display. To implement the electrically coupled indirect view system for high-end applications, microdisplay with high resolution, power efficiency, reliability and other merits must be addressed. Of the two categories of microdisplays [33], modulating microdisplays, such as liquid crystal on silicon (LCOS) or digital light processor (DLP) based, are relatively matured in technology, driven by the commercial markets of project TV and other applications. These modulating microdisplays are blanket-illuminated by separated light sources and modulate incident light on a pixel-by-pixel basis, with intrinsic low power efficiency. In addition, the field-of-view, brightness and contrast of these modulation-based microdisplays are far less than desired for applications such as under direct sunlight or under extreme conditions. The other category is emissive microdisplays, which should provide high power efficiency; a critical requirement for portable near-to-eye (NTE) head mounted systems or dismounted mobile systems and hand-held projector systems, especially for the field applications. Currently, the maturing technology of emissive microdisplay is based on colour-filtered organic LED (OLED) technology. Although significant progress has been achieved in the OLED field in the last 20 years, the electro-optical performance, power efficiency and lifetime of OLED itself are still inferior to its inorganic counterpart LED. OLEDs suffer not only from a shorter life span but also from nonuniform degradation of luminance for various colours over their lifespan. Furthermore, a full-colour OLED microdisplay with high resolution based on side-by-side patterned RGB sub-pixels has not been demonstrated and is currently based on filtering of broadband white emitters, with approximately more than 2/3 of the white OLED output removed by the filter to obtain the required RGB primary colours. For example, up to 90% of the optical power from the white OLED has to be filtered out to obtain a sufficiently saturated red sub-pixel, so the OLED must be driven up to be ten times brighter than the required pixel brightness, which substantially shortens the lifetime of the microdisplay. Degradation is further enhanced by the heat generation from filters.

Other possible candidates for emissive microdisplays include, for example, the inorganic electroluminescent (EL) microdisplays based on phosphor materials [34], porous silicon microdisplay [35], carbon nanotube (CNT) based field-emission (FE) microdisplay [36] and indium gallium nitride (InGaN) μ -emitter arrays originally developed by the authors [12]. Technically speaking, EL microdisplay is relatively matured, but the high voltage requirement limits its further development. The efficiency of porous silicon is far away from real applications. CNT-based microdisplay is still in the

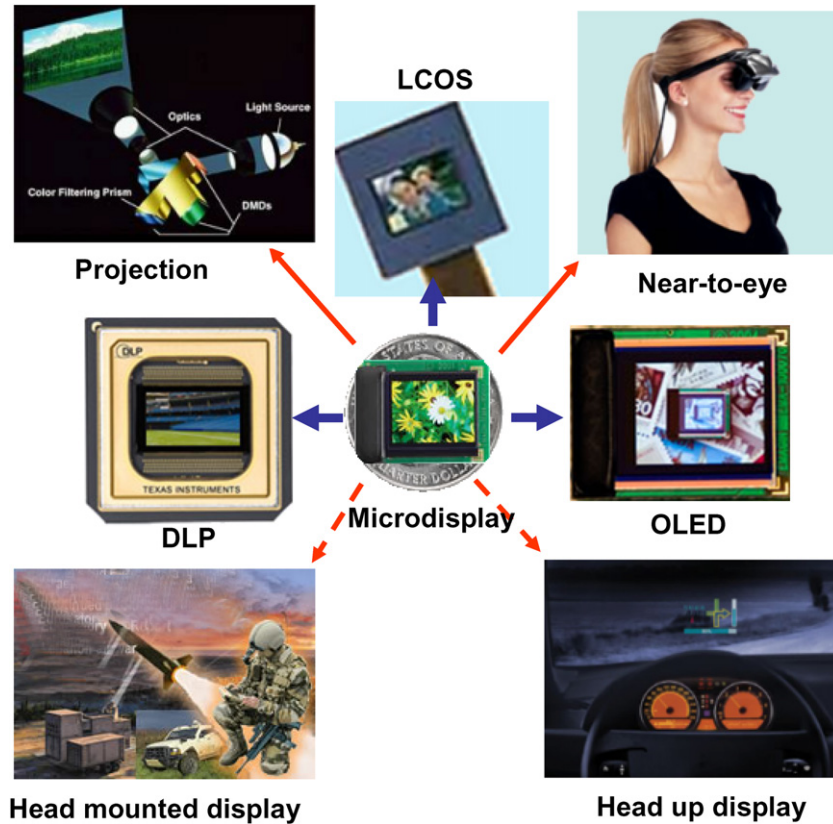


Figure 6. Coin-size microdisplays have two categories of applications: projection or near-to-eyes. The current technologies are based on LCOS, DLP and OLED, and all of them have limitations in brightness, efficiency and robustness, especially for applications such as head-up displays used in a car running under sunlight, or head-mounted displays used in the extreme condition of field applications (Image sources: <http://www.ti.com>, <http://www.emagin.com>, <http://www.siemensvdo.com>).

early research stage. Of all the possible options, the well-developed semiconductor emitter array, with its intrinsic power efficiency, reliability, colour purity and other merits, could be a better candidate for the accomplishment of next-generation high performance full-colour microdisplay.

In the last twenty years, high brightness LEDs (HB-LEDs) based on InGaN and AlGaInP semiconductors have achieved dramatic development with the driving for indicating and solid-state lighting applications. InGaN emitters have efficiency several times higher than OLEDs, electroluminescent emitters and other emitters. With the quantum-well structures, LEDs have a narrow emission band of about 25 nm, providing a basis for high colour purity and chromatic fidelity. With their intrinsic material properties and low voltage operation characteristics, LEDs have a much longer operational lifetime (>100 000 h), can be operated at extreme conditions such as high or low temperature (-50° to 120°) and humidity and can be easily driven by the CMOS silicon drivers without high voltage requirement. They can provide a viewing angle of more than 120° . All these intrinsic properties render them an ideal candidate for display applications.

Matrix addressable microdisplay has two driving schemes. For low information content microdisplay with resolution below 160×120 pixels, passive driving by X–Y scanning is widely used because of its convenience and low cost while for high resolution microdisplay, active driving based on each driving cell corresponding to each pixel is a preferred scheme to

ensure the frame refreshing. Depending on the driving scheme, the design of the μ LED array is also different.

5.1. Passive-driven μ LED array

For passive-driven design, each μ LED pixel is connected with an anode on the column data line and a cathode on the row scan line. When a specific row is scanned, the brightness of each pixel on this row is decided by its column data line which provides a current corresponding to the pixel brightness (grey scale) to turn this pixel on. The basic μ LED array structure is shown in the schematic diagram of figure 7. The top view of figure 7(a) shows the X–Y matrix layout, with the n-line bus connecting all the cathodes of LEDs in the X direction (row) and the p-line bus connecting all the anodes of LEDs in the Y direction (column). The n-line bus is composed of the n-contact metal wire on n-GaN, while the p-line bus is formed by metal deposition; between the n-line and the p-line is a silicon oxide isolation layer. Figure 7(b) is the cross-section view along the p-line, showing the details of the processing steps. Each row of pixels can be isolated from each other by a deep trench of $2 \mu\text{m}$ width and $3\text{--}5 \mu\text{m}$ depth.

The deep trench may influence the pixel performance uniformity and the device yield. Choi *et al* [37] demonstrated that by controlling the ICP plasma etching conditions such as plasma power, plate power and pressure, the mesa structure may be etched with an isotropic recipe to achieve

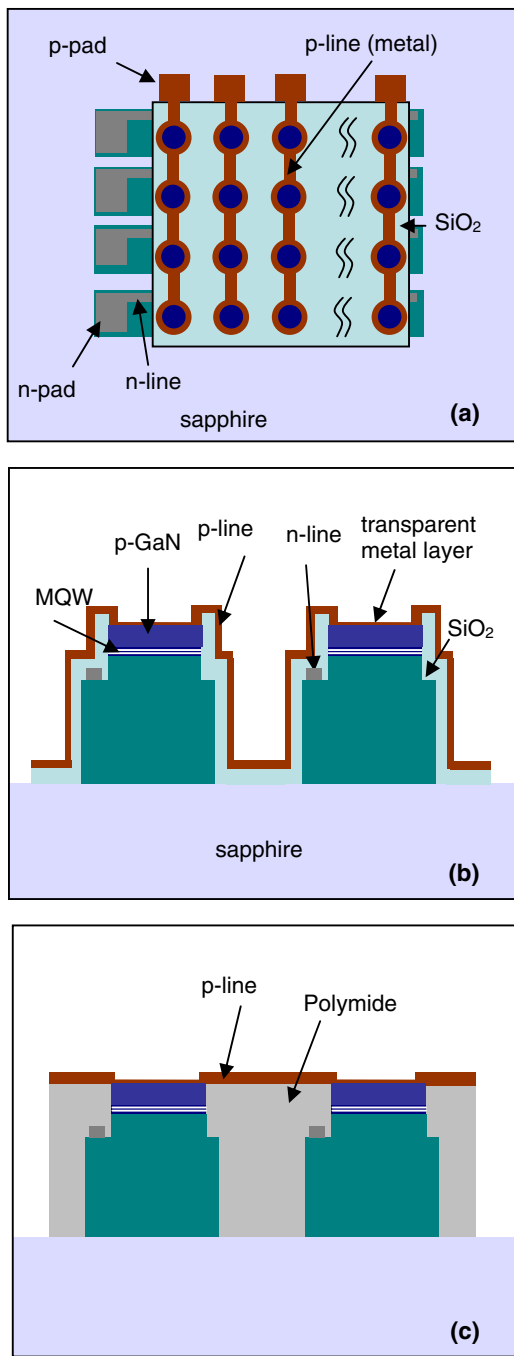


Figure 7. (a) The top view and (b) the cross-section view of the schematic diagrams of the passive-driven microdisplay. (c) The cross-section view after surface planarization.

tapered sidewalls, so that the isolation layer and the metal interconnection can be conformably deposited on the uneven surface. However, this approach will increase the trench width and decrease the filling factor of pixels. Surface planarization based on the chemical and mechanical polishing (CMP) process was also demonstrated. SiO₂ is deposited to fill the deep trenches, and then the dielectric layer on p-GaN is selectively removed by CMP with a special slurry, which selectively removes SiO₂ without attacking GaN [38]. Unfortunately, the polishing will unavoidably introduce defects in the GaN and its current spreading layer,

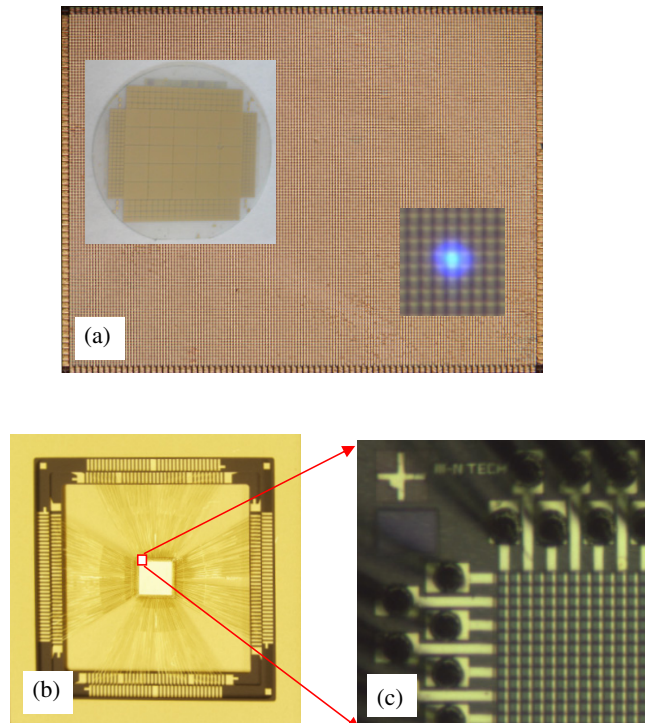


Figure 8. Microscope images of a (a) 160 × 120 microdisplay fabricated by the authors with inset showing the processed 2 in. wafer and one pixel turned on, (b) a 120 × 120 microdisplay device with a die size of 3.2 mm × 3.2 mm is encapsulated in the standard 281-pin PGA package and (c) the zoom-in image shows the device and wire bonding (courtesy: III-N Technology, Inc.).

increasing the non-radiative recombination centres. The cross-section view after surface planarization based on polyimide is schematically shown in figure 7(c).

A microdisplay with 160 × 120 pixels and a pixel pitch of 22 μm fabricated in the authors' laboratory is shown in figure 8(a), with the inset showing the processed 2 inch wafer. After wafer thinning and die singularity, the device is packed in a PGA package with wire bonding, shown in figures 8(b) and (c). For the 1/4 QVGA format μLED array with a pixel size of 20 × 12 μm and a pixel pitch of 22 μm, figure 9 shows the characterization of an individual μLED, which has a broad current range covering several scales from sub-micrometre ampere up to milli-ampere, with a potential to achieve a highly bright microdisplay with a high grey scale. The pixel also has a wide viewing angle of more than 120°. The blue μLED has a peak wavelength of 470 nm with the FWHM of 30 nm; at a driving voltage of 3.2 V, it has a current of 10 μA with a power output of 0.25 μW. This corresponds to a wall-plug efficiency of 0.78% for a 20 × 12 μm² pixel. The luminous efficacy should be calculated from the spectra characteristics of the LED emission. As an estimation, assuming the pixel's 470 nm emission has a negligible FWHM, the luminous efficacy will be around 60 lm W⁻¹. This value is only 8% of the peak value (683 lm W⁻¹) of the photonic curve which occurs at 555 nm. If the InGaN based green LED wafer with an emission wavelength of around 520 nm is used for microdisplay, the luminous efficacy can be dramatically improved by one order.

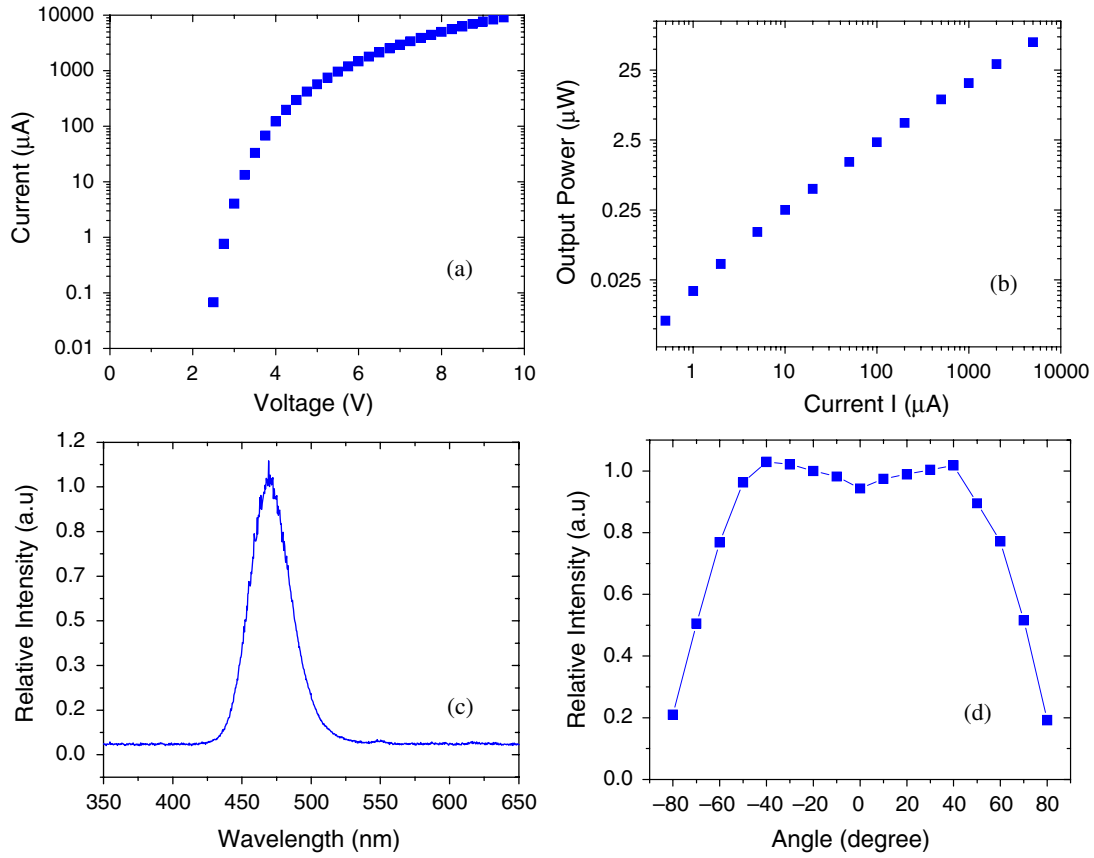


Figure 9. The μ LED pixel characterization of (a) I - V , (b) L - I , (c) spectrum and (d) viewing angle.

Based on the luminous efficacy value and the pixel L - I characteristics, the luminance properties of a fully illuminated passive-driven μ LED array can be estimated from the equation [39]

$$L_V = (pK)/(N_R D^2), \quad (1)$$

where L_V is the luminance in foot-lambert (fL), p the pixel output power (W), K the luminance efficacy (lm W^{-1}), N_R the number of rows in the array which are scanned and D the pixel pitch in the array (feet). The total current for the μ LED array is given by

$$I = N_C i, \quad (2)$$

where N_C is the number of columns in the array and i is one pixel drive current.

Based on the pixel characterization in figure 9, it is estimated that for the above 1/4 QVGA (160×120) array, at a pixel current of $10 \mu\text{A}$, the microdisplay has a luminance of more than 20 fL at a total current of 1.6 mA. Assuming a 3.2 V forward bias for each pixel at $10 \mu\text{A}$, the power dissipation within the μ LED array is only 5.1 mW. If a green wavelength is used for microdisplay, the luminance can be roughly increased by one order of magnitude under similar power dissipation. It should be pointed out that in the motion picture industry, the recommended light output is 16 fL for commercial movie theatres with no film in the projector, and in the flight simulation industry, the peak display luminance (screen brightness) for full flight simulators (FFS) is specified

as no less than 6 fL. To achieve a peak luminance of 20 fL, the InGaN based microdisplay only dissipates about 5 mW, well below the maximum ratings of battery power supplies of most portable electronic products, and the low power dissipation ensures extended operating duration. The almost linearity of the L - I characteristics of μ LED also shows that the pixels are capable of emitting much greater light for virtual display at a higher input power. This capability predicts that the InGaN μ LED has a great potential for larger display formats and use in applications requiring high brightness, for example, handheld projectors used outdoors. In [16], Choi *et al* reported 128×96 nitride blue and green microdisplays with 1200 dpi, as shown in figure 10. With an injection current of 60 mA at a voltage ~ 5 V, 3.3 mW and 2.4 mW of power is emitted from the blue and green microdisplays, respectively, corresponding to a luminance of $\sim 30\,000 \text{ Cd m}^{-2}$, significantly higher than OLED microdisplays, which have a luminance of $\sim 1000 \text{ Cd m}^{-2}$ at 5 V.

To connect a μ LED array with hundreds of pins to passive driver/controller IC chips under the restriction of minimizing the microdisplay module size, flip-chip bonding is the suitable approach, in which the chip-on-glass (COG) driver and μ LED array device both are directly bonded on board through gold bumps, and the connections between driver and array are implemented through the photolithography defined metal wires on the board. One prototyping board we are working on is shown in figure 11, in which an off-the-shelf OLED segment/common driver with controller is used to drive the μ LED array.

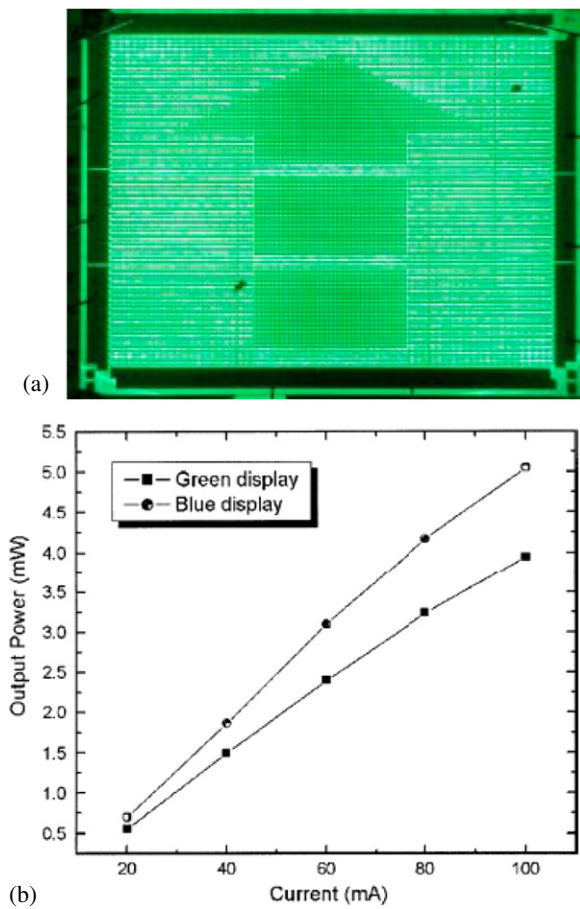


Figure 10. (a) The image of one green microdisplay showing an arrow pattern and (b) $L-I$ characteristics of the blue and green microdisplays (after [14]).

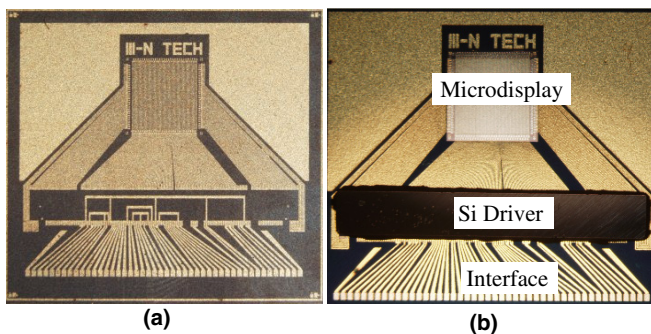


Figure 11. A compact module design based on flip-chip bonding of a μ LED array and a Si driver IC on the same board. Photographs of (a) the board without chips and (b) after flip-chip bonding of the μ LED array and the Si chip (courtesy: III-N Technology, Inc.).

5.2. Active driven μ LED array

The above monolithic microdisplay based on III-nitride μ LED arrays connected with a separated driving circuit can be driven only in the passive mode. For an array format more than QVGA (320×280), to ensure the refreshing frequency and pixel brightness, the μ LED array should be designed for active driving with each pixel corresponding to a driving unit. The schematic of a driving unit cell is shown in figure 12(a), in which each μ LED pixel shares a common cathode ground

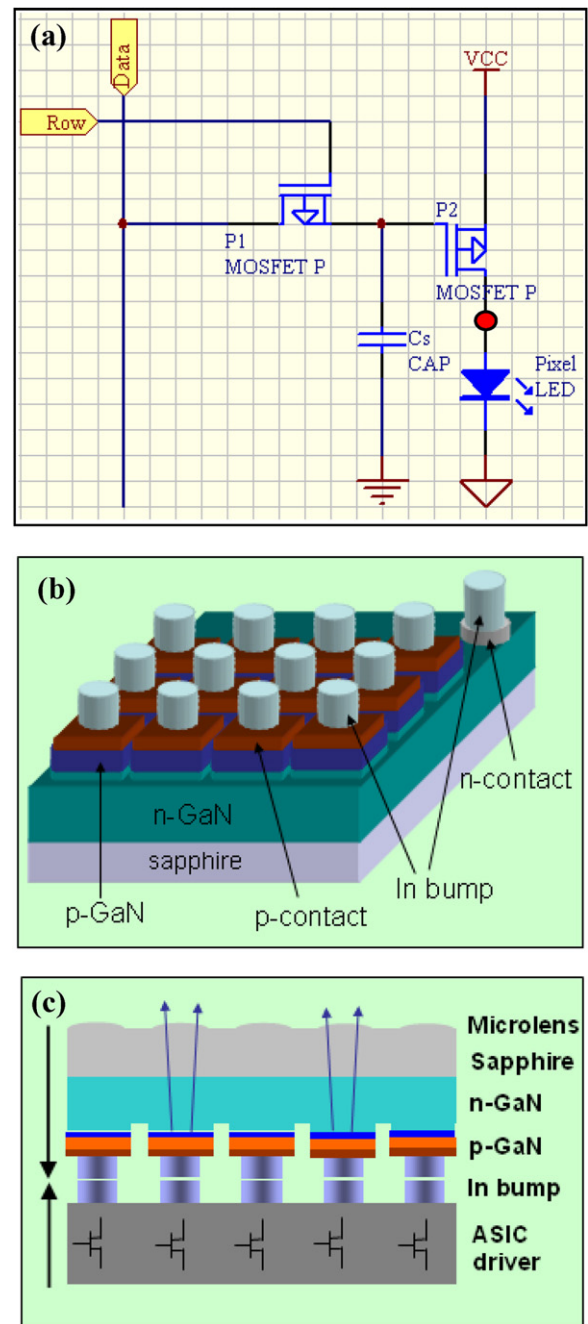


Figure 12. (a) Circuit schematic of an active driving unit cell. (b) The structure of a μ LED array for active driving. (c) Integration of a μ LED array with Si IC by flip-chip bonding for active driving.

with an independent anode connected with its driving transistor based on the silicon CMOS IC. Since a nitride μ LED array cannot be directly fabricated on Si IC, hybrid integration is necessarily based on flip-chip bonding. Figures 12(b) and (c) show the schematic structure of the hybrid LED microdisplay. Compared with passive driving, the design and fabrication of the μ LED array are simplified. Without etching down to sapphire to form the isolated n-GaN strips, all μ LEDs in the array now have their n-GaN layers connected together, and all the p-contacts are left open with the indium bumps and will be bonded to driving transistors on Si IC. All μ LEDs have a common n-contact, and p-line buses are removed. By

removing the interconnected n- and p-metal bus lines and the related large isolation space, the light emitting area can be designed to be close to the pixel area, so the filling factor can be dramatically improved from less than 40% to more than 80%, comparable to LCD technology. With a high filling factor, the III-nitride microdisplay can deliver a seamless image without the pixelation phenomenon.

6. Micro-emitter array based microarray biochips

Fluorescence spectroscopy, sensing and imaging, with its merits of high sensitivity down to single molecular level, specificity, nondestructive nature and *in situ* sample compatibility, is a powerful tool in the biology and molecular chemistry research. Traditionally, the light source for fluorescence is either the bulky high-pressure mercury or xenon lamps or expensive gas or solid-state lasers. The recently developed AlInGaN-based light emitters, depending on the material composition, provide a tunable wavelength in the range from green and blue to UV and deep UV, an ideal light source for fluorescence spectroscopy studies. Compared with bulk lamps and gas/solid-state lasers, AlInGaN light emitters have a compact size and cheap price, easily integrated to construct portable detection instruments. They can be pulsed on the sub-nanosecond timescale [17], very suitable for fluorescence decay measurement. The development of AlGaIn deep UV emitters with the wavelength below 300 nm is especially unique. Other light sources with enough power at this wavelength are not easily available, and this spectrum range is critical for protein and cell study.

In the literature, III-nitride LEDs with different wavelengths have been investigated as a light source for fluorescence study. McGuinness *et al* have a series of publications using subnanosecond AlGaIn-based DUV LEDs at 295 nm [40], 280 nm [41] and 265 nm [42] for the protein fluorescence decay time study. The Brown/Yale group [43, 44] has used an individual-addressable UV LED linear array with wavelength between 340 and 280 nm as a light source, to study the spectroscopic finger printing of airborne biological particles, with NADH (with absorption at 340 nm) or amino acids tryptophan (with absorption at 280 nm) as probes. Figure 13(a) is the image of the flip-chip bonded UV LED array they used with each LED having a dimension of $50\ \mu\text{m} \times 200\ \mu\text{m}$. Figure 13(b) shows the real-time fluorescence channel recordings for a single NADH particle with two concentration levels.

Many applications of an UV/DUV μLED array for bio-sensing can be envisaged. As one example, we will illustrate the chip-scale integrated label-free detection of proteins based on their intrinsic fluorescence. As a powerful tool for genomic study, DNA microarray is based on fluorophore-labelled fluorescence for a comparative gene expression analysis or DNA resequencing. The very success of the DNA microarray has also boosted the development of array and microarray based biochips and sensors as indispensable and high-throughput tools for genomics and proteomics study and disease diagnostic. As the workhorse of cells, the understanding of proteins is vital for disease development

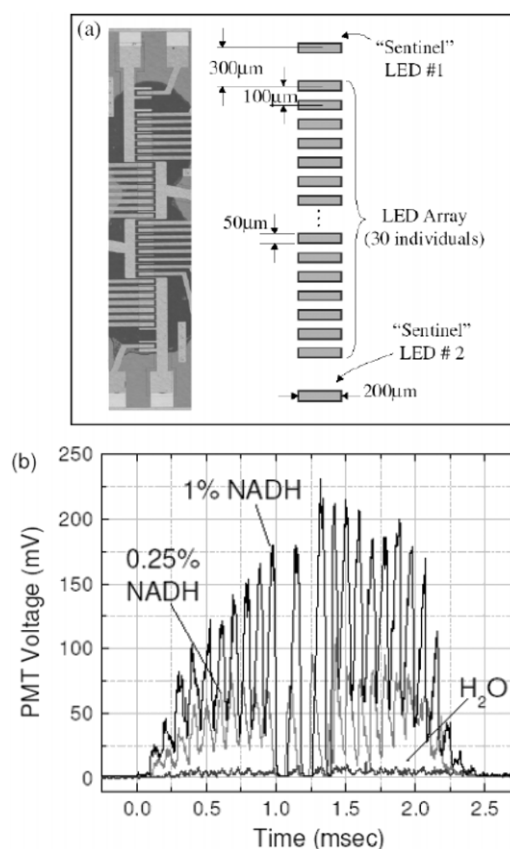


Figure 13. (a) Photograph and device layout of the 32-element UV LED array and (b) real-time fluorescence channel recordings for single NADH particles with two concentrations (after [43]).

monitoring and drug design. There has been growing interest in developing a protein microarray [45], with the potential that protein functions such as enzyme activity, antibody specificity and other ligand–receptor interactions, as well as the binding of nucleic acid or small molecules to proteins, can all be analysed. Unlike in the DNA microarray where the probes are fluorescently labelled to detect the hybridization intensity, labelling detection of protein has several drawbacks, such as changing proteins' natural activity, labelling efficiency variation and time-consuming [46]. A great deal of effort is now concentrated on label-free detection of proteins [47] based on traditional optical (surface plasma resonance), acoustic (quartz crystal resonator) and calorimetric (isothermal titration calorimetry) and novel approaches such as scanning nanoprobe and nanowires [48].

DNA has too weak an intrinsic fluorescence to be useful, but the three aromatic amino acids in protein—phenylalanine (Phe), tyrosine (Tyr), and tryptophan (Trp)—are all fluorescent when excited in the 260–300 nm DUV region [49], of which tryptophan is the dominant intrinsic fluorophore, absorbing 280 nm deep UV light and emitting fluorescence light at around 350 nm. In recent years, AlGaIn-based 280 nm and shorter wavelength DUV light emitters have been achieved [50, 51], providing a portable light source for protein intrinsic fluorescence study and detection. Based on the DUV μLED array, a chip-scale integrated label-free protein array detection system could be constructed. The DUV emission from each

μ LED pixel is coupled onto a corresponding binding spot on the sensing array, and the fluorescence from each binding spot on the sensing array is collected by the detector array through a bandpass filter. From the intrinsic fluorescence intensity measurement, the protein concentrations on the different spots may be detected. Such a compact system may be developed into a portable biosensor for point-of-care testing. Based on the same approach, the DNA microarray detection instrument may also be constructed by using a μ LED array as a fluorescence excitation source, with each μ LED pixel corresponding to a hybridization position on the DNA microarray for parallel excitation, and the image is recorded by the CCD camera or other detector arrays.

7. Summary

Based on the concept and development of nitride μ -emitters, several emerging technologies based on μ -emitter arrays have been realized and envisioned. With serial connection, the authors have achieved μ LED array based single-chip ac-LEDs which can be directly driven by high ac line voltage. The single-chip ac-LED technology is completely compatible with current lighting and electricity infrastructures and is expected to bring the concept of SSL much closer to reality and create new lighting applications previously not imagined. With parallel connection, the authors have realized an interconnected μ LED that provides higher extraction efficiency than its broad-area LED counterpart. With matrix addressable connection based on passive driving or active driving, μ LED arrays have been utilized to build high brightness emissive microdisplays. Nitride μ -emitter, with its wavelength tunable from the visible to the DUV range, will find many applications in microarray biosensors based on fluorescence excitation and detection. More efforts are still needed to develop full-colour microdisplays and III-nitride μ -emitter array based microarrays for biological and medical applications.

Acknowledgments

Our research programme is supported by grants from NSF, ARO, DOE and DARPA. This invited paper is a collection of contributions from our current and former group members. The authors specially acknowledge the contributions of Dr J Li, Dr S X Jin and Ms W P Zhao.

References

- [1] Mair R A, Zeng K C, Lin J Y, Jiang H X, Zhang B, Dai L, Tang H, Botchkarev A, Kim W and Morkoc H 1997 Optical properties of GaN/AlGaIn multiple quantum well microdisk *Appl. Phys. Lett.* **71** 2898–900
- [2] Mair R A, Zeng K C, Lin J Y, Jiang H X, Zhang B, Dai L, Botchkarev A, Kim W, Morkoc H and Khan M A 1998 Optical modes within III-nitride multiple quantum well microdisk cavities *Appl. Phys. Lett.* **72** 1530–2
- [3] Zeng K C, Dai L, Lin J Y and Jiang H X 1999 Optical resonance modes in InGaIn/GaN multiple-quantum-well microring cavities *Appl. Phys. Lett.* **75** 2563–5
- [4] Lee J W et al 1996 Etching processes for fabrication of GaN/InGaIn/AlN microdisk laser structure *J. Vac. Sci. Technol. B* **14** 3637–40
- [5] Akasaka T, Kobayashi Y, Ando A and Kobayashi N 1997 GaN hexagonal microprisms with smooth vertical facets fabricated by selective metalorganic vapor phase epitaxy *Appl. Phys. Lett.* **71** 2196–8
- [6] Bidnyk S, Little B D, Cho Y H, Karasinski J, Song J J, Yang W and McPherson S A 1998 Laser action in GaN pyramids grown on (1 1 1) silicon by selective lateral overgrowth *Appl. Phys. Lett.* **73** 2242–4
- [7] Zeng K C, Lin J Y, Jiang H X and Yang W 1999 Optical properties of GaN pyramids *Appl. Phys. Lett.* **74** 1227–9
- [8] Li X, Bohn P W, Kim J, White J O and Coleman J J 2000 Spatially resolved band-edge emission from partially coalesced GaN pyramids prepared by epitaxial lateral overgrowth *Appl. Phys. Lett.* **76** 3031–3
- [9] Chang S, Rex N B, Chang R K, Chong G and Guido L J 1999 Stimulated emission and lasing in whispering-gallery modes of GaN microdisk cavities *Appl. Phys. Lett.* **75** 166–8
- [10] Jiang H X, Lin J Y, Zeng K C and Yang W 1999 Optical resonance modes in GaN pyramid microcavities *Appl. Phys. Lett.* **75** 763–5
- [11] Jin S X, Li J, Li J Z, Lin J Y and Jiang H X 2000 GaN microdisk light emitting diodes *Appl. Phys. Lett.* **76** 631–3
- [12] Jiang H X, Jin S X, Li J, Shakya and Lin J Y 2001 III-nitride blue microdisplays *Appl. Phys. Lett.* **78** 1303–5 *US Patent* 6,410,940
- [13] Ozden I, Diagne M, Nurmikko A V, Han J and Takeuchi T 2001 A matrix addressable 1024 element blue light emitting InGaIn QW diode array *Phys. Status Solidi. a* **188** 139–42
- [14] Choi H W, Jeon C W and Dawson M D 2004 High-resolution 128 \times 96 nitride microdisplay *IEEE Electron Device Lett.* **25** 277–9
- [15] Jeon C W, Choi H W, Gu E and Dawson M D 2004 High-density matrix-addressable AlInGaIn-based 368 nm microarray light-emitting diodes *IEEE Photon. Technol. Lett.* **16** 2421–3
- [16] Wu S, Chhajed S, Yan L, Sun W H, Shatalov M, Adivarahan V and Khan M A 2006 Matrix addressable micro-pixel 280 nm deep UV light-emitting diodes *Japan. J. Appl. Phys.* **45** L352–4
- [17] Jin S X, Li J, Shakya J, Lin J Y and Jiang H X 2001 Size dependence of III-nitride microdisk light emitting diode characteristics *Appl. Phys. Lett.* **78** 3532–4
- [18] Choi H W, Jeon C W, Dawson M D, Edwards P R, Martin R W and Tripathy S 2003 Mechanism of enhanced light output efficiency in InGaIn-based microlight emitting diodes *J. Appl. Phys.* **93** 5978–82
- [19] Jiang H X, Lin J Y and Jin S X 2005 Light-emitting diodes for high AC voltage operation and general lighting *US Patent* No 6957899
- [20] Fan Z Y, Jiang H X and Lin J Y 2007 Heterogeneous integrated high voltage DC/AC light emitters *US Patent* No 7,221,044
- [21] Egawa T, Ohmura H, Ishikawa H and Jimbo T 2002 Demonstration of an InGaIn-based light-emitting diode on an AlN/sapphire template by metalorganic chemical vapor deposition *Appl. Phys. Lett.* **81** 292–4
- [22] Li J, Lin J Y and Jiang H X 2006 Growth of III-nitride photonic structures on large area silicon substrates *Appl. Phys. Lett.* **88** 171909
- [23] Kramer M R 1999 High-power truncated-inverted-pyramid $(\text{Al}_x\text{Ga}_{1-x})_{0.5}\text{In}_{0.5}\text{P}/\text{GaP}$ light-emitting diodes exhibiting >50% external quantum efficiency *Appl. Phys. Lett.* **75** 2365–7
- [24] Schnitzer I, Yablonovitch E, Caneau C, Gmitter T J and Scherer A 1993 30% external quantum efficiency from surface textured, thin-film light-emitting diodes *Appl. Phys. Lett.* **63** 2174

- [25] Khizar M, Fan Z Y, Kim K H, Lin J Y and Jiang H X 2005 Nitride deep-ultraviolet light-emitting diodes with microlens array *Appl. Phys. Lett.* **86** 173504
- [26] Oder T N, Kim K H, Lin J Y and Jiang H X 2004 III-nitride blue and ultraviolet photonic crystal light emitting diodes *Appl. Phys. Lett.* **84** 466
- [27] Jin S X, Li J, Lin J Y and Jiang H X 2000 InGaN/GaN quantum well interconnected microdisk light emitting diodes *Appl. Phys. Lett.* **77** 3236–8
- [28] Choi H W, Jeon C W and Dawson M D 2003 InGaN light emitting diodes of micro-ring geometry *Phys. Status Solidi. c* **0** 2185–8
- [29] Nam K B, Li J, Nakarmi M L, Lin J Y and Jiang H X 2004 Unique optical properties of AlGaN and related ultraviolet emitters *Appl. Phys. Lett.* **84** 5264–6
- [30] Kim H, Li J, Jin S X, Lin J Y and Jiang H X 2003 III-nitride ultraviolet light-emitting diodes with delta doping *Appl. Phys. Lett.* **83** 566–8
- [31] Adivarahan V, Wu S, Sun W H, Mandavilli V, Shatalov M S, Simin G, Yang J W, Maruska H P and Khan M A 2004 High-power deep ultraviolet light-emitting diodes based on a micro-pixel design *Appl. Phys. Lett.* **85** 1838–40
- [32] Wu S, Adivarahan V, Shatalov M, Chitnis A, Sun W H and Khan M A 2004 Micro-pixel design miliwatt power 254 nm emission light emitting diodes *Japan. J. Appl. Phys.* **43** L1035–7
- [33] Armitage D, Underwood I and Wu S T 2006 *Introduction to Microdisplays* (Chichester: Wiley)
- [34] Aguilera M, Arbutnot L and Keyser T 1996 First generation VGA electroluminescent display for head-mounted applications *Proc. SPIE* **2735** 92
- [35] Smirnov A, Labunov V and Lazarouk S 2005 Si-based LED microdisplay: design and manufacturing process *Proc. IDRC* **25** 474
- [36] Fusayasu T, Tanaka Y, Kasano K, Fukuda H, Song P and Kim B 2005 Development of a microdisplay based on the field emission display technology *Lecture Note Comput. Sci.* **3824** 1036–44
- [37] Choi H W, Jeon C W and Dawson M D 2005 Tapered sidewall dry etching process for GaN and its application in device fabrication *J. Vac. Sci. Technol. B* **23** 99–102
- [38] Jeon C W, Choi H W and Dawson M D 2003 Fabrication of matrix-addressable InGaN-based microdisplays of high array density *IEEE Photon. Technol. Lett.* **15** 1516–8
- [39] Holm P, Rhyne W, Gable B, Rogers S P, Jachimowicz, Richard F and Ackley D E 1999 Two-dimensional LED arrays for virtual display image sources *IEEE Trans. Electron. Devices* **46** 897–904
- [40] McGuinness C D, Sagoo K, McLoskey D and Birch D J S 2005 Selective excitation of tryptophan fluorescence decay in proteins using a subnanosecond 295 nm light-emitting diode and time-correlated single-photon counting *Appl. Phys. Lett.* **86** 261911
- [41] McGuinness C D, Sagoo K, McLoskey D and Birch D J S 2004 A new sub-nanosecond LED at 280 nm: application to protein fluorescence *Meas. Sci. Technol.* **15** L19–22
- [42] McGuinness C D, Macmillan A M, Sagoo K, McLoskey D and Birch D J S 2006 Excitation of fluorescence decay using a 265 nm pulsed light-emitting diode: evidence for aqueous phenylalanine rotamers *Appl. Phys. Lett.* **89** 063901
- [43] Davitt K, Song Y K, Nurmikko A V, Jeon S R, Gherasimova M, Han J, Pan Y L and Chang R K 2004 UV LED arrays for spectroscopic fingerprinting of airborne biological particles *Phys. Status Solidi c* **2** 2878–81
- [44] Davitt K, Song Y K, Patterson W, Nurmikko A V, Ren Z, Sun Q and Han J 2007 UV LED arrays at 280 and 340 nm for spectroscopic biosensing *Phys. Status Solidi a* **204** 2112–6
- [45] Kambhampati D 2004 *Protein Microarray Technology* (Weinheim: Wiley)
- [46] Haab B B 2003 Methods and applications of antibody microarrays in cancer research *Proteomics* **3** 2116–22
- [47] Cooper M A 2003 Label-free screening of bio-molecular interactions *Anal. Bioanal. Chem.* **377** 834–42
- [48] Stern E, Klemic J F, Routenberg D A, Wyrembak P N, Turner-Evans D B, Hamilton A D, LaVan D A, Fahmy T M and Reed M A 2007 Label-free immunodetection with CMOS-compatible semiconducting nanowires *Nature* **445** 519–22
- [49] Lakowicz J R 1999 *Principles of Fluorescence Spectroscopy* 2nd edn (New York: Plenum)
- [50] Nakarmi M L, Kim K H, Khizar M, Fan Z Y, Lin J Y and Jiang H X 2005 Electrical and optical properties of Mg-doped Al_{0.7}Ga_{0.3}N alloys *Appl. Phys. Lett.* **86** 092108
- [51] Khan M A, Shatalov M, Maruska H P, Wang H M and Kuokstis E 2005 III-nitride UV devices *Japan. J. Appl. Phys.* **44** 7191–206